

Cooperative symmetry-breaking by actin polymerization in a model for cell motility

Alexander van Oudenaarden*† and Julie A. Theriot‡§

*Department of Chemistry, Stanford University, Stanford, California 94305, USA

†Present address: Department of Physics, Massachusetts Institute of Technology, Cambridge, Massachusetts 02139, USA

‡Department of Biochemistry and Department of Microbiology and Immunology, Stanford University, Stanford, California 94305, USA

§e-mail: theriot@cmgm.stanford.edu

Polymerizing networks of actin filaments are capable of exerting significant mechanical forces, used by eukaryotic cells and their prokaryotic pathogens to change shape or to move. Here we show that small beads coated uniformly with a protein that catalyses actin polymerization are initially surrounded by symmetrical clouds of actin filaments. This symmetry is broken spontaneously, after which the beads undergo directional motion. We have developed a stochastic theory, in which each actin filament is modelled as an elastic brownian ratchet, that quantitatively accounts for the observed emergent symmetry-breaking behaviour. Symmetry-breaking can only occur for polymers that have a significant subunit off-rate, such as the biopolymers actin and tubulin.

A central problem in cell biology lies in understanding how small-scale biochemical interactions generate large-scale organization and cellular structure. Most eukaryotic cells are structurally polarized, and the establishment and maintenance of their polarity depends on anisotropic organization of their cytoskeletal elements¹. In multicellular organisms, cell polarity is often influenced by external signals, but many cell types are capable of spontaneously breaking symmetry and generating well-defined structural polarity in the absence of extrinsic spatial cues².

Actin is a major cytoskeletal protein of eukaryotic cells, which binds and hydrolyses ATP and self-assembles to form long helical filaments^{3,4}. Actin polymerization into filaments can produce significant mechanical force^{5,6}. Protrusive motility in biological systems can be initiated by local catalysis of actin polymerization, for example at the leading edge of lamellipodia and filopodia in crawling (amoeboid) cells^{7,8}. Persistent directional cell locomotion requires an asymmetric distribution of growing actin filaments, a classic example of cell polarity^{9–11}. Similar to polymerization at the leading edge of amoeboid cells, local polymerization of actin filaments is also catalysed at the surface of some intracellular bacterial

pathogens, including *Listeria monocytogenes*, *Shigella flexneri* and spotted-fever group *Rickettsia*¹². Host-cell actin polymerization pushes these bacteria through the cytoplasm, enabling efficient intracellular and intercellular spread^{13–16}. For *L. monocytogenes*, actin polymerization is induced by the virulence factor ActA, a bacterial surface protein¹⁷. ActA interacts with host-cell proteins to catalyse local actin-filament nucleation¹⁸ and elongation¹⁹, but ActA does not remain physically attached to the filaments. As with amoeboid actin-based motility, persistent directional motion in the bacterial systems requires an asymmetric distribution of growing actin filaments. Shortly after entering the host-cell cytoplasm, *L. monocytogenes* becomes surrounded by a symmetric ‘cloud’ of host-cell actin filaments. Movement is initiated when the symmetric cloud is rearranged to form an asymmetric ‘tail’¹³. The ActA protein is distributed in a polarized fashion on the bacterial surface, and its distribution dictates which pole will form the tail²⁰.

Here, we explore how actin asymmetry arises and is maintained, starting from a symmetric filament distribution. We have studied the process of symmetry-breaking in an *in vitro* system, in which the polarized bacterium is replaced with a spherical polystyrene bead

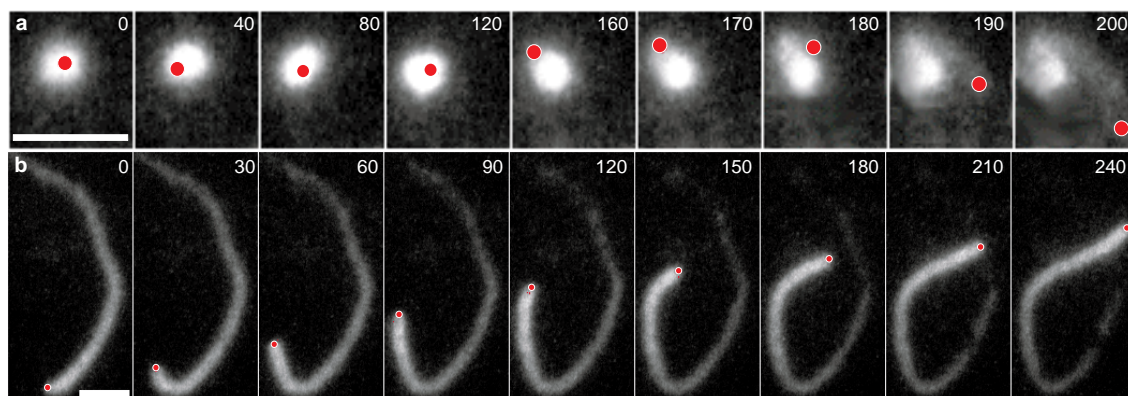


Figure 1 Symmetry-breaking in a cloud of actin filaments. Time sequence of combined phase-contrast and fluorescence microscopy images of an actin cloud that spontaneously breaks symmetry (a), and a bead propelled by polymerizing filaments after symmetry-breaking (b). The bead shown in b moves with a constant velocity of

0.12 $\mu\text{m s}^{-1}$. The grey scale shows the fluorescence intensity of rhodamine-labelled actin. The actual position of the bead is monitored using phase-contrast microscopy and is represented by the red circle. The scale bars denote 5 μm . Time elapsed is shown in seconds.

that has no structural asymmetry, and have compared experimental measurements with the predictions of a new theoretical model that is based on the known dynamic properties of actin polymerization. We find that the presence of the bead effectively couples the polymerization of different filament tips, such that filaments on the same side of the bead cooperate with one another, while filaments on opposite sides of the bead inhibit each other's growth. This arrangement allows for small stochastic fluctuations to be amplified under certain conditions, so that symmetry-breaking can readily occur for the system as a whole. The coupling between polymerization dynamics and mechanical force in a system of interacting actin filaments can explain the actin cytoskeleton's remarkable ability to act as a self-organizing system capable of spontaneously generating unidirectional motion.

Results

Symmetry-breaking of an actin 'cloud' *in vitro*. We have purified a soluble derivative of the *L. monocytogenes* ActA protein in which the transmembrane anchor has been replaced with a hexahistidine tag¹⁸. We added carboxylated polystyrene beads uniformly coated with purified ActA-His to *Xenopus laevis* egg cytoplasmic extract supplemented with fluorescently labelled actin monomers^{21,22}. After a brief incubation (<15 min), symmetric clouds of actin filaments are observed around the beads (see, for example, Fig. 1a at $t=0$ s). Neighbouring filaments are crosslinked to one another by actin-binding proteins present in the cytoplasmic extract²³, forming a dense cloud around the bead. Filaments in this cloud are initially nucleated at the surface of the bead^{14,16,18}, and elongate by intercalation of a new actin monomer between an existing filament end and the bead surface. Initially, this elongation pushes the filament away from the bead surface, but, when the crosslinked shell is fully formed, filament movement is constrained so that elongation of filament tips at the bead surface can no longer push the filament away from the bead. Instead, the polymerizing filaments start to exert mechanical forces on the bead. At this point (typically after >1 h of incubation), a spontaneous symmetry-breaking of the actin cloud is frequently observed.

An example of a bead for which symmetry-breaking occurs is depicted by the time sequence in Fig. 1a. At $t=0$ s, the bead was surrounded by a dense symmetric actin cloud. Before $t=0$ s, the position of the bead did not change within the resolution of the phase-con-

trast microscope. Between $t=0$ s and $t=160$ s, however, the bead started to make small random excursions inside the cloud (Fig. 1a). At $t=170$ s, a striking instability occurred: the bead jumped out of the cloud and started to move with a constant velocity of $\sim 0.12 \mu\text{m s}^{-1}$, leaving an empty actin cloud and a comet-like tail of polymerized crosslinked actin in its wake. With this asymmetric actin distribution, beads can move persistently for many minutes at constant velocity (Fig. 1b). This type of motility is very similar to that observed for *L. monocytogenes*^{14,15,21}.

Theoretical model for symmetry-breaking. We wished to determine the minimal theoretical requirements for a system to exhibit the spontaneous symmetry-breaking observed experimentally (Fig. 1a). An elastic brownian ratchet model has been proposed⁵ to link elongation of a single actin filament to force generation. In this mean-field model, different filaments are assumed to be independent: all filaments grow with the same speed and exert the same force. This mean-field approach is not valid in our experimental system because the presence of the bead couples the dynamics of different filaments. We therefore developed a new stochastic theory that models the filaments around the bead as a collective system of interacting brownian ratchets (Fig. 2). The filaments are constrained to be perpendicular to the bead surface and are spaced uniformly around its circumference (Fig. 2a). A necessary condition for elongation at the tip of the filament is that the size of the gap between the tip and the bead surface be large enough for intercalation of an actin subunit (the minimum gap size, Δ , is ~ 2.7 nm, or half the diameter of an actin subunit, because the filament is made up of two staggered protofilaments)³. Considering the actin filaments as elastic rods (Fig. 2b), we derive the probability P_{on} for subunit addition to the free end of a filament. The functional form of the probability $P_{\text{on}}(x)$ is plotted in Fig. 2c. As actin polymerization is a reversible reaction, there is also a significant probability that a growing filament will lose its terminal subunit²⁴. We therefore introduce a finite depolymerizing probability, P_{off} , that is independent of x . For simplicity in the calculations, we normalize $P_{\text{on}}=1$ at $x=\Delta$. The relative value of P_{off} is determined by the kinetic rate constants for polymerization and depolymerization of actin: $P_{\text{off}}=k_{\text{off}}/(k_{\text{on}}M)$, where M is the concentration of actin monomer available for polymerization at the bead surface. Using these assumptions, we performed stochastic calculations that predict the time-dependent behaviour of a bead that started with an ideal symmetric distribution of N filaments at $t=0$.

The main observations resulting from the stochastic calculations are summarized in Figs 3–5. Figure 3a shows an example of a calcu-

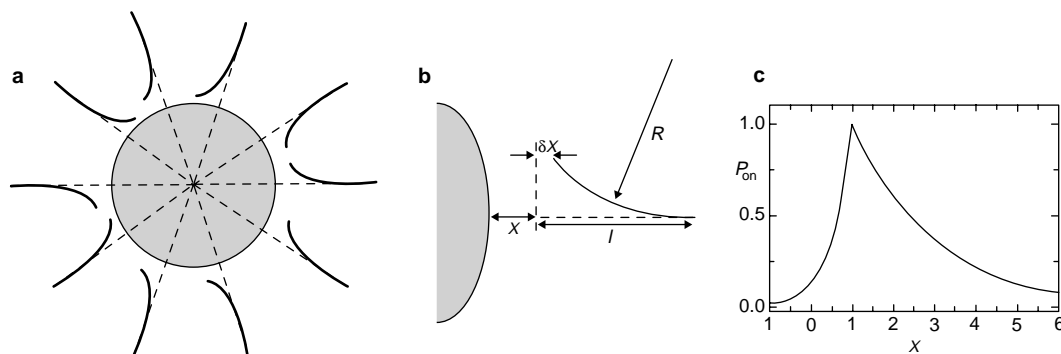


Figure 2 Description of the multifilament stochastic model. a, Initial symmetric distribution of actin filaments around a bead. The filaments are assumed to be orientated perpendicular to the bead surface and are evenly spaced. **b,** Each actin filament is considered as an elastic rod with length l . The tip-bead distance for a non-bent filament is given by x . Because of thermal fluctuations, the end of an actin filament that is close to the bead surface can bend, which increases the bead-tip distance by δx . The other end of the filament is fixed in space because of crosslinking with other filaments. For small deflections, the filament bends with a constant radius of curvature R . **c,** The probability of subunit addition, P_{on} , is a function of distance x . Note that all distances are normalized to the size of the gap Δ required to permit intercalation of

an actin monomer between the filament tip and the bead surface ($\Delta \approx 2.7$ nm)³. A necessary condition for subunit addition to the free end is that the gap opened between the fluctuating tip and the bead surface be large enough to allow a monomer to intercalate: $x + \delta x \geq 1$. For $x < 1$, the probability that this condition be met can be calculated from Boltzmann's distribution for thermal bending. Experimentally, actin polymerization has been seen to be confined to the immediate vicinity of the bacteria or bead surface^{14,16}. This is represented by introducing an exponential decay of $P_{\text{on}}(x)$ for $x > 1$. $P_{\text{on}}(x)$ is maximal at $x = 1$, where the filament tip is at the position closest to the bead that allows actin-monomer intercalation without filament bending. See Methods for details.

lated trajectory for a bead surrounded by $N=50$ filaments with a small likelihood of losing a terminal subunit, $P_{\text{off}}=0.02$. This trajectory is compared with a two-dimensional random walk (Fig. 3b) computed for identical step sizes. Note that the total path length of the two trajectories is identical. The random walk (Fig. 3b) can

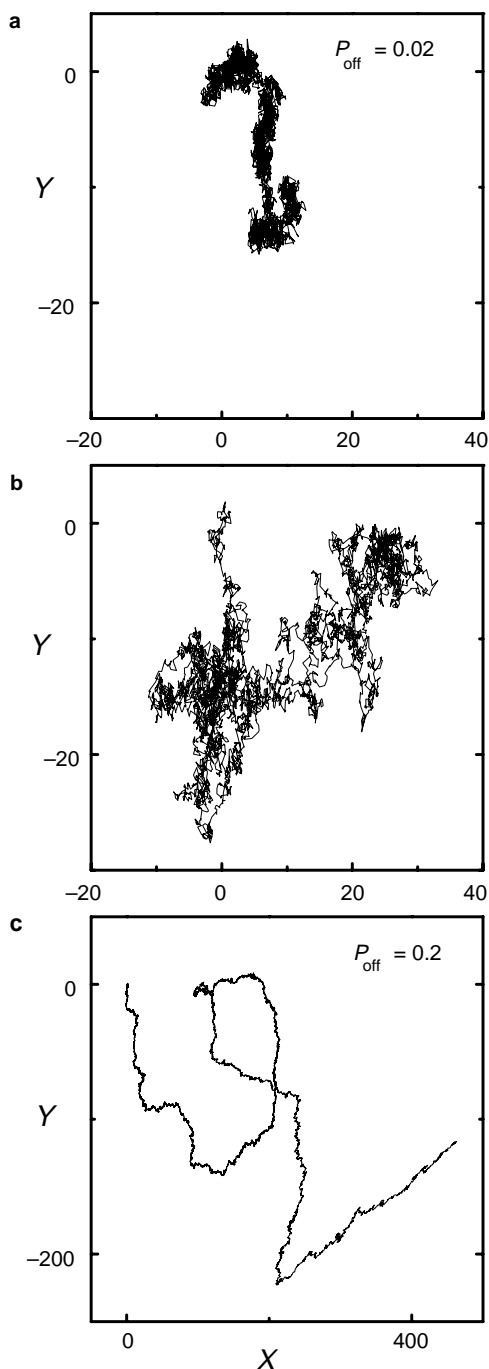


Figure 3 Examples of bead trajectories calculated using the stochastic model.

a, Obstructed random walk for a bead surrounded by 50 rarely depolymerizing filaments ($P_{\text{off}}=0.02$), compared with **b**, a conventional random walk. The bead starts its trajectory at $X=0$ and $Y=0$, where X and Y are the two spatial coordinates normalized to the minimum gap size Δ . Note that the total path distance covered in **a**, **b** is the same, but the filaments obstruct the net motion of the bead. **c**, Directional motion of bead with filaments having a moderate depolymerization probability $P_{\text{off}}=0.2$. Note the change in scale with respect to the trajectories shown in **a**, **b**. The trajectories were obtained after 25,000 iterations.

explore a larger area in a given time than the bead surrounded by filaments: the actin filaments around the bead obstruct the net movement. Surprisingly, the opposite behaviour is observed for beads that are surrounded by filaments from which subunit loss is a more likely occurrence. Compared with random walk (Fig. 3b), a bead surrounded by filaments with $P_{\text{off}}=0.2$ can traverse a significantly larger net distance, although the total path length (and therefore the amount of energy consumed) remains the same (Fig. 3c; note change in scale). In this regime the filaments amplify the motion of the bead. The moderate values of P_{off} where motion amplification is observed are consistent with the known rate constants for addition and loss of actin subunits from filaments under physiological conditions near steady state^{4,24}. We conclude that the readily reversible nature of actin-filament polymerization enables a specific and biologically important aspect of actin-based cell motility, the ability of polymerizing actin networks to amplify random motion and effectively convert it into directed motion.

To examine how this behaviour evolves over time, we plotted the variance of r , the net displacement of the bead, averaged over 100 independent calculated trajectories as a function of the number of iterations i (Fig. 4a). Note that the number of iterations i is proportional to time t . For $i < 10^2$, the beads exhibit a subdiffusive motion independent of P_{off} : $\langle r^2 \rangle \propto t^p$, where the power $p < 1$. For these short times the beads are caged by the actin clouds, which are still fairly symmetric. However, for $P_{\text{off}}=0.2$ and $i > 10^2$, the beads exhibit a superdiffusive motion: $\langle r^2 \rangle \propto t^p$, where the power $p \approx 2$ (depicted by the dashed line in Fig. 4a). This value indicates that the beads undergo unidirectional motion. The transition from subdiffusive to superdiffusive behaviour shifts to smaller i values for increasing values of P_{off} . This time-dependent behaviour, where beads undergo a period of a confined random walk followed by a sudden transition to unidirectional motion, is strikingly similar to our experimental observation (Fig. 1a).

To make a quantitative comparison of this theoretical prediction with our experimental results, we have plotted $\langle r^2 \rangle$, averaged over seven observed experimental trajectories, versus time t (Fig. 4b). We determined the variance $\langle r^2 \rangle$ using trajectories of beads just before they escape from the actin cloud (for example, $0 < t < 180$ s in Fig. 1a), while they are still completely surrounded by actin filaments and the

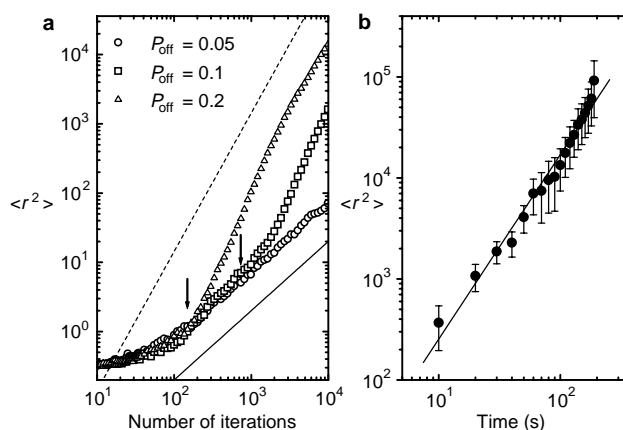


Figure 4 Time-dependent subdiffusive and superdiffusive motion.

a, Variance $\langle r^2 \rangle$ as a function of the number of iterations for three different values of P_{off} . The variance is computed from averaging over 100 bead trajectories. The solid line depicts the slope for conventional two-dimensional diffusion: $\langle r^2 \rangle \propto t$, whereas the dashed line represents unidirectional motion: $\langle r^2 \rangle \propto t^2$. The arrows indicate the transition from diffusive to superdiffusive behavior. **b**, Experimentally obtained variance $\langle r^2 \rangle$ versus time, computed by averaging over seven trajectories of beads recorded before escaping from the actin cloud. A power law was fitted with a superdiffusive characteristic: $\langle r^2 \rangle \propto t^{1.8}$. Distances were normalized to the minimum gap size Δ (2.7 nm).

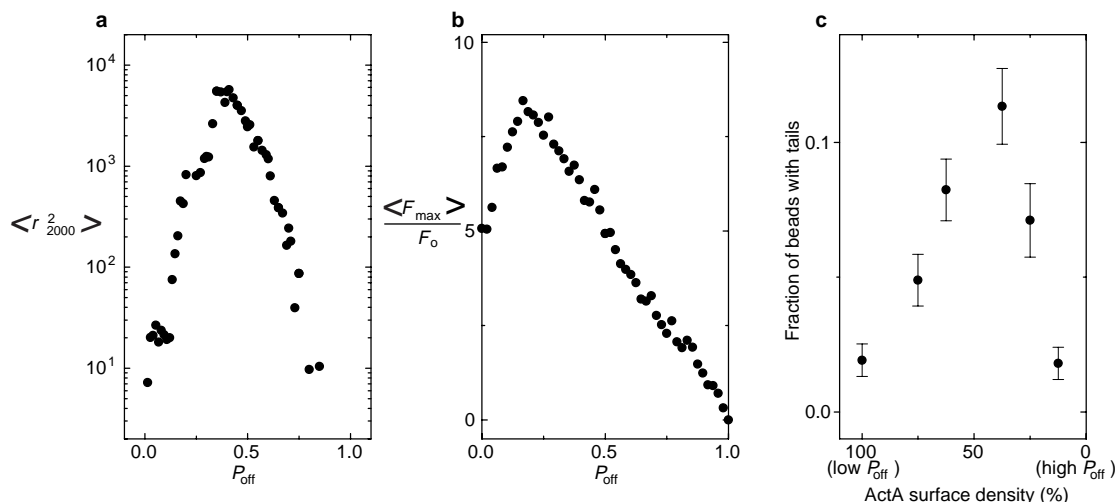


Figure 5 Influence of P_{off} on distance travelled, force generated, and likelihood of escape from the actin cloud. **a**, Variance $\langle r_{2000}^2 \rangle$ after 2,000 iterations as a function of P_{off} (averaged over 20 calculated trajectories). For all the stochastic calculations, $N = 50$ and $P_{\text{on}}(x)$ is given by the function shown in Fig. 2. **b**, Maximum net force on bead versus P_{off} . The maximum force F_{max} is determined in

the interval $1 < i < 2,000$, where i is the iteration number, and then averaged over 20 independent stochastic calculations. **c**, Experimental dependence of tail formation on ActA surface density; P_{off} is inversely related to ActA density. Data in **c** are taken from ref. 22.

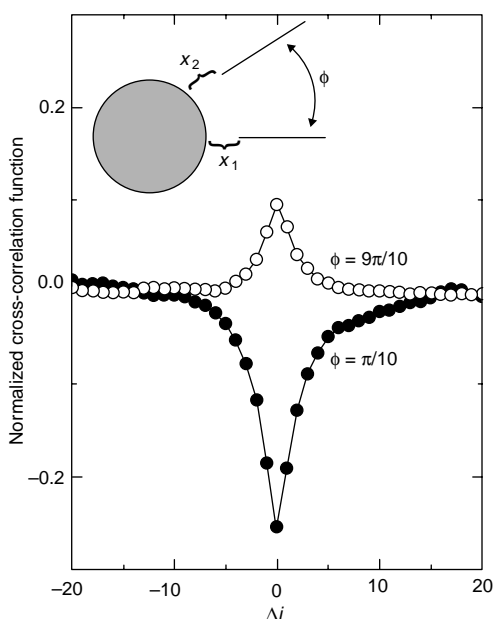


Figure 6 Cooperativity between filaments. Inset (top), the simplified two-filament model. Two filaments perpendicular to the bead surface are separated by an angle ϕ , with gaps between the filament tips and the bead surface designated x_1 and x_2 . Calculations were performed as for the 50-filament model, and the tip-bead distances for both filaments were tracked as a function of the iteration number, i . The cross-correlation function $\langle x_1(i)x_2(i + \Delta i) \rangle$ normalized to the autocorrelation $\langle x_1^2(i) \rangle$ is plotted as a function of Δi for two different values of ϕ . The graph shows that a negative correlation is observed for the small angle $\phi = \pi/10$, indicating that the filaments interact cooperatively in a hand-over-hand fashion, with the addition of a subunit to one filament opening a gap that enhances the likelihood of elongation of the other filament. The positive correlation for the large angle $\phi = 9\pi/10$ indicates that the elongation of one filament interferes with the elongation of the other. The correlations are averaged over 100 independent stochastic calculations.

assumptions of the model are valid. Distance moved is normalized to the minimum gap size Δ (2.7 nm), allowing a direct comparison between the calculated and observed trajectories. The beads within

their actin clouds exhibit a superdiffusive motion characterized by the power law $\langle r^2 \rangle \propto t^{1.8}$, in good agreement with the predicted behaviour for $P_{\text{off}} = 0.2$. Unfortunately we cannot access the subdiffusive regime for short times because the excursions of the beads in this regime are smaller than the resolution of the phase-contrast microscope, which is about 50 nm, corresponding to $\langle r^2 \rangle \approx 400$.

To demonstrate explicitly the influence of P_{off} on the distance travelled by the beads, we plotted the variance $\langle r_{2000}^2 \rangle$ after 2,000 iterations versus P_{off} , averaged over 20 calculated trajectories (Fig. 5a). A maximum variance is observed near $P_{\text{off}} \approx 0.4$. For $P_{\text{off}} \ll 0.4$, the actin filaments rarely shrink and therefore obstruct the motion of the bead; the bead is caged by the actin cloud (Fig. 3a). For $P_{\text{off}} \gg 0.4$, the filaments tips rarely grow. After a small number of iterations all filament tips are outside the ActA-catalysing range ($P_{\text{on}}(x) \rightarrow 0$), leaving a static bead behind. Similarly, we calculated the influence of P_{off} on the magnitude of the force experienced by the bead. In our stochastic model the maximum net force exerted on the bead reaches a maximum value of about $8F_0$ near $P_{\text{off}} \approx 0.2$ (Fig. 5b), where $F_0 \approx 3.1$ pN is the magnitude of the force exerted by a single filament acting as an elastic brownian ratchet⁵. Note that if all filaments were concentrated on only one hemisphere of the bead, the net force would be $NF_0/\pi \approx 16F_0$. Therefore, the observed value of $8F_0$ implies that the initially symmetric filament cloud has become significantly asymmetric after 2,000 iterations with $P_{\text{off}} \approx 0.2$.

This prediction of the model, that movement and force generation will be most efficient at intermediate values of P_{off} can also be confirmed experimentally. As seen in Fig. 1a, the bead breaks out of the actin cloud, which forms a tail, when the net force on the bead is larger than the confining force of the crosslinked actin cloud. The frequency of tail formation should therefore be correlated with the amount of force experienced by a bead under a given experimental condition. We can vary P_{off} by changing the surface density of ActA on the beads; because ActA catalyses filament growth, high ActA surface densities correspond to low values of P_{off} and vice versa (although we cannot predict the exact functional form of P_{off} dependence on ActA surface density, it is likely to be nonlinear). Experimentally, we observe that tail formation is more likely at intermediate ActA surface densities than at either high or low densities (Fig. 5c)²², qualitatively consistent with the model's prediction of an optimal $P_{\text{off}} \approx 0.2-0.4$, where the most net force is generated and the transition to unidirectional movement occurs most rapidly.

Is P_{off} actually within this critical range in our experimental sys-

tem? Remember that $P_{\text{off}} = k_{\text{off}}/(k_{\text{on}}M)$. For addition of ATP-bound actin to the barbed (rapidly growing) end of a filament, $k_{\text{off}} \approx 1 \text{ s}^{-1}$ and $k_{\text{on}} \approx 5 \mu\text{M}^{-1} \text{ s}^{-1}$ (refs 4, 24). We can estimate M at the bead surface from the velocity of beads that have broken symmetry and are moving under a condition of low load (Fig. 1b), using $v = \Delta M k_{\text{on}} - \Delta k_{\text{off}}$. For $v = 0.12 \mu\text{m s}^{-1}$, $M \approx 9 \mu\text{M}$. This gives $P_{\text{off}} \approx 0.02$, where spontaneous symmetry-breaking is not predicted. However, the presence of a moveable load such as a bead at the tip of a growing filament effectively increases P_{off} by altering the ratio between k_{on} and k_{off} (ref. 25). Under compressing force, $P_{\text{off}}(\text{loaded}) = P_{\text{off}}(\text{unloaded}) \exp(\Delta F/k_{\text{B}}T)$, where F is the magnitude of the load force²⁵. Using $F \approx 3.5 \text{ pN}$ will raise P_{off} by about tenfold, so that $P_{\text{off}}(\text{loaded}) \approx 0.2$. This modest force is similar to the force that can be exerted by a single filament tip ($\approx 3.1 \text{ pN}$; see above). The model thus indicates that the compression of individual filaments because of generation of tension in a crosslinked cloud is a necessary prerequisite to symmetry-breaking. This prediction resolves a long-standing experimental puzzle. Although *L. monocytogenes* or ActA-coated beads in host-cell cytoplasm or cytoplasmic extracts generate symmetric clouds within 15–30 min, movement is not initiated until 1–1.5 h (refs 13, 21, 22). We conclude that the long incubation time is required for sufficient tension to be generated to compress the growing filaments and increase P_{off} to values at which symmetry-breaking is possible. It is not clear whether this tension may be regulated in some way to maintain P_{off} within the optimal range of 0.2 to 0.4. How the load-dependence of P_{off} quantitatively affects the process of symmetry-breaking will be a subject of our forthcoming work.

The spontaneous symmetry-breaking that we observe in the model indicates that the actin filaments in the cloud may behave cooperatively, such that the addition or loss of a subunit on one actin filament influences the likelihood of addition or loss on other filaments. To demonstrate this explicitly using our stochastic model, we considered a bead propelled by only two filaments normal to the bead surface, separated by an angle ϕ . In Fig. 6 the cross-correlation function $\langle x_1(i)x_2(i+\Delta i) \rangle$ is shown, where $x_1(i)$ and $x_2(i)$ are the tip–bead distances at iteration number i , and Δi is an increment of iteration number. If the behaviour of the filaments were independent, the cross-correlation would be zero: the tip–bead distance of one filament would have no influence on the tip–bead distance of the other filament at any time point. Instead, we observe that filaments that are almost parallel ($\phi = \pi/10$) are anti-correlated (Fig. 6, black dots). If, at a given time, one filament tip is closer to the bead than its average position, it is significantly likely that the other filament tip will be further from the bead than its average position. The filaments therefore operate cooperatively in a hand-over-hand fashion: addition of a subunit to one filament tip pushes the bead forward, generating a gap which enables efficient addition of a subunit to the other filament tip. As expected, the cooperativity is strongly dependent on ϕ . For filaments that are almost anti-parallel ($\phi = 9\pi/10$) a positive cross-correlation is observed (Fig. 6, white dots) and the filaments interfere with each other's growth. In this geometry, addition of a subunit to the tip of one filament nudges the bead slightly closer to the tip of the other filament, inhibiting the second filament's growth.

In this simplified two-filament model we have, therefore, explicitly demonstrated that subunit addition and loss on one filament strongly affect the behaviour of another filament. It is this coupling among the dynamic behaviours of different filaments that results in the emergent symmetry-breaking and superdiffusive behaviour we have observed in the multifilament calculations (Figs 3–5).

Discussion

In biological systems, all forms of protrusive actin-based motility are mediated by large populations of actin filaments rather than by individual filaments acting alone. Our stochastic model extends previous single-filament calculations⁵ to demonstrate explicitly how the presence of a load can couple the dynamics of individual

filaments under tension to produce an emergent symmetry-breaking behaviour. The type of symmetry-breaking we describe here has been observed for a variety of spherically symmetric particles where actin polymerization is catalysed at the particle surface, including beads coated with the *L. monocytogenes* protein ActA²², beads coated with the mammalian proteins WASP²⁶ or N-WASP (S. J. McCallum and J.A.T., unpublished observations), and lipid vesicles containing phosphatidylinositol-4,5-bisphosphate²⁷. As the symmetry-breaking process appears to be qualitatively similar in all these cases, we conclude that symmetry-breaking is a general property of actin-filament dynamics and is not dependent on the detailed molecular mechanism of catalysis at the particle surface. We have found that two properties of actin filaments are particularly critical for efficient symmetry-breaking in a system in which forces are generated by protein polymerization.

First, it is necessary that the polymerization reaction be readily reversible, that is, that the subunit off-rate at a growing filament tip be moderately high. Intuitively it is straightforward to understand why bead movement will be inefficient in the two limiting cases, where P_{off} is close to 0 or close to 1. If the subunit off-rate is small ($P_{\text{off}} < 0.05$) symmetry-breaking cannot occur, because the filaments all are constantly growing and cage the bead inside a symmetric cloud. In this regime, the bead performs a random walk with a step size that is much smaller than the actin-subunit size Δ . Conversely, if P_{off} is large ($P_{\text{off}} > 0.8$), the filaments will quickly depolymerize away from the surface of the bead, and the bead will then undergo a diffusive random walk whose step size is determined by the diffusion coefficient of the bead. The surprising emergent behaviour of symmetry-breaking and superdiffusive movement appears only for intermediate values of P_{off} , most efficiently when $P_{\text{off}} \approx 0.2$ – 0.4 (Figs 4, 5). In this range, some filaments will grow while others shrink. Because addition of a subunit to one filament will increase the probability of addition of a subunit to nearby filaments (Fig. 6), the simultaneous growth of near neighbours is positively reinforced. Conversely, addition of a subunit to one filament will inhibit the addition of a subunit to filaments that are on the opposite side of the bead (Fig. 6). It is difficult to predict what the collective behaviour of multiple filaments exerting these positive and negative influences on one another will be. Intuitive reasoning is limited and the full dynamics of this complex stochastic system is revealed only by performing numerical simulations that take into account all of the interactions between the randomly growing and shrinking filaments. Our calculations have revealed that, in this regime, small stochastic variations in filament growth are amplified, resulting in large-scale superdiffusive movement. The requirement of a significant subunit off-rate for symmetry-breaking is uniquely fulfilled by biopolymers such as actin and tubulin, for which the individual subunits are held together by weak noncovalent bonds; most synthetic polymers and other biopolymers such as DNA are held together by covalent bonds, which do not show the required degree of reversibility. Although much previous work has focused on the importance of nucleotide hydrolysis in the complex dynamic behaviour of actin filaments and microtubules, the significance of their relatively weak subunit–subunit contacts has not, to our knowledge, been explored previously.

The second requirement for symmetry-breaking in our system is the generation of compressive tension in the filaments. Given the high concentrations of polymerizable actin monomers in eukaryotic cells, the absolute value of P_{off} is comparatively low, and it is necessary that the actin filaments be under a compressive load before symmetry-breaking can become efficient. The fact that polymerization kinetics are sensitive to mechanical force²⁵ provides a mechanism for coupling the dynamic behaviour of filaments that are physically distant from one another in the cell, allowing small-scale biochemical interactions to generate large-scale cellular asymmetry.

Cooperative symmetry-breaking by populations of dynamic actin filaments has been frequently observed in whole-cell motility. The special case we have described, of ActA-coated beads, can be

translated into the more general case of initiation of actin-based amoeboid cell motility by a simple geometrical inversion; in our system, actin filaments point inwards and exert force on a bead at the centre, while in most forms of cell motility actin filaments point outwards and exert force on the limiting plasma membrane. Many cell types use polarized actin-based motility to crawl up concentration gradients of chemoattractants. Cells that are exposed to a uniform concentration of chemoattractant will spontaneously polarize and move persistently in a random direction²⁸. Thus the chemoattractant signal appears to impart a preferred directionality to the cell's cytoskeletal asymmetry, but the establishment and maintenance of asymmetry itself is a function of the inherent dynamics of the actin cytoskeleton. An even more striking example of spontaneous symmetry-breaking is provided by lamellipodial fragments from fish epithelial cells²⁹. These fragments typically assume a non-polarized, non-motile disc shape, but will occasionally break symmetry, adopt a polarized shape reminiscent of the whole cell, and move persistently. The transition from the symmetric to the asymmetric actin distribution can be triggered experimentally by a mechanical nudge³⁰. In these two cases, it is clear that the influence of the external polarizing signal imparts only a choice of direction, and is not required for establishment or maintenance of large-scale cellular asymmetry itself.

It is likely that many types of cellular symmetry-breaking follow this general rule. One well-characterized example is the generation of the anteroposterior axis in the frog (*Xenopus laevis*) embryo. The egg is cylindrically symmetric, and after fertilization symmetry is broken by a microtubule-dependent rotation of the cortex relative to the cytoplasm. The direction of this cortical rotation and hence the position of the animal's primary body axis is determined by an external signal, the sperm entry point. However, an artificially activated egg (with no sperm entry point) will perform a cortical rotation in an apparently random direction and, if later injected with a sperm nucleus and centrosome, will develop into a normal embryo³¹. In this case, self-assembly of microtubules to form an asymmetric large-scale structure appears to be intrinsic to the system, and the signal once again imparts only the choice of direction rather than the asymmetry *per se*. The dynamic behaviours of cytoskeletal polymers, in particular the reversibility of polymerization and the sensitivity of polymerization to mechanical stresses, have apparently been fine-tuned through evolution to optimize their collective ability to break symmetry at the cellular scale, a robust intrinsic property that can be triggered by spatial cues in the cell's environment but can also develop spontaneously. □

Methods

Motility assays.

Carboxylated polystyrene beads of 0.5 μm in diameter (Polysciences, Inc.) were incubated for 1 h in a solution of 1 mg ml⁻¹ hexahistidine-tagged ActA¹³ and 1 mg ml⁻¹ ovalbumin in *Xenopus* extract buffer (XB: 100 mM KCl, 0.1 mM CaCl₂, 2 mM MgCl₂, 5 mM EGTA, 10 mM potassium HEPES, pH 7.7). Beads were rinsed in XB and added to *X. laevis* egg cytoplasmic extract supplemented with 0.15 mg ml⁻¹ tetramethylrhodamine iodoacetamide-labelled actin²⁵. Motility assays were performed as described²². The surface density of ActA-His was varied by changing the ratio of ActA-His and ovalbumin, keeping the total protein concentration constant. Time-lapse video microscopy was done using a Nikon Diaphot-300 inverted microscope and an intensified charge-coupled-device (CCD) camera (Dage-MTI GenIISys/CCD-c72), collecting paired phase-contrast and epifluorescence images at 10-s intervals. Particle tracking and digital image analysis were done using Metamorph (Universal Imaging Corporation, Media, PA) software. Every image was recorded by averaging over eight video frames.

Stochastic model.

The model starts with a bead with an ideal symmetric distribution: $x = 0.5$ for all N filaments. Each actin filament is considered as an elastic rod with length l and bending modulus B . The tip-bead distance for a non-bent filament is given by x . As a result of thermal fluctuations, the end of an actin filament that is close to the bead surface can bend, which increases the bead-tip distance by δx . The other end of the filament is fixed in space as a result of crosslinking with other filaments. Filaments are constrained to be perpendicular to the bead surface, which leads to a bending energy $E \propto \delta x$. For actin filaments that are orientated under an angle $\theta \gg \sqrt{2l/(9\lambda)}$ with respect to the bead surface $E \propto \delta x^2$, which alters $P_{on}(x)$. Qualitatively, no significant differences between the results of the stochastic calculations for a linear and a quadratic bending energy were observed. For small deflections, the filament bends with a constant radius of curvature R and δx is given by $l - R \sin(l/R) \approx l/(6R)$. The bending energy of a filament is given by $E = B/l(2R^2) \approx 3B\delta x/l$. The bending modulus B can be approximated by $B \approx \lambda k_B T$, where λ is the persistence length of an actin filament (a measurable property describing the distance that must be

travelled along a filament before the tangent vectors become uncorrelated), k_B is Boltzmann's constant, and T is the absolute temperature. Distances are normalized to the size of the gap Δ required to permit intercalation of an actin monomer between the filament tip and the bead surface ($\Delta \approx 2.7 \text{ nm}$)³. A necessary condition for subunit addition to the free end³ is $x + \delta x \geq 1$. The probability $P_{on}(x)$ that a sufficiently large gap opens to allow an extra subunit to add onto the filament tip is given by: $P_{on}(x) = \int_{1-x}^1 \exp(-E/k_B T) d(\delta x) = \exp(-1-x/L_1)$, where $L_1 = l/(3\delta\Delta)$. The length of a filament¹³ $\approx 200 \text{ nm}$ and the persistence length³²⁻³⁵ $\lambda \approx 10 \mu\text{m}$ lead to $L_1 \approx 0.5$, which characterizes the exponential decay for $x < 1$. Actin polymerization is confined to the region immediately adjacent to the particle surface^{14,16}, perhaps because filament capping is suppressed by close proximity to the ActA protein^{37,38}. This effect is phenomenologically modelled by introducing an exponential decay of $P_{on}(x)$ for $x > 1$ with a characteristic length L_2 , which is the approximate length of the ActA protein²⁰; $L_2 \approx 2 \cdot P_{on}(x)$ is normalized to 1 at $x = 1$. Varying the value of L_2 does not significantly change the outcome of the calculations. P_{on} is assumed to be independent of x , and is a constant between 0 and 1.

To compute the time-dependent behaviour of a bead we used the following stochastic algorithm. To decide whether a filament grows, a random number γ_1 between 0 and 1 is generated. If $\gamma_1 < P_{on}(x)$, this filament grows by one subunit. If $\gamma_1 \geq P_{on}(x)$, no addition occurs. This stochastic decision is performed for each filament. After determining whether each filament adds one subunit, we generate a second random number γ_2 to determine whether the filament shrinks by one subunit: if $\gamma_2 < P_{off}$ the filament loses one subunit but if $\gamma_2 \geq P_{off}$ no loss occurs. Next, the total elastic energy resulting from bending of filaments, $U = \sum_i E_i$, is calculated as a function of the bead position. The bead is now moved to that position for which U is minimized. If there are multiple positions with the same lowest energy, the bead is moved to that position for which its displacement is smallest. Finally, the new tip-bead distances x for each filament are updated with respect to the new bead position and the whole procedure is iterated. Computations were performed on a Hewlett Packard work station. For the stochastic decisions, we used a long-period random-number generator of L'Ecuyer with Bays-Durham shuffle.

RECEIVED 15 JUNE 1999; REVISED 13 OCTOBER 1999; ACCEPTED 20 OCTOBER 1999; PUBLISHED 8 NOVEMBER 1999.

1. Drubin, D. G. & Nelson, W. J. Origins of cell polarity. *Cell* **84**, 335-344 (1996).
2. Bornens, M. Cell polarity: intrinsic or externally imposed? *New Biol.* **3**, 627-636 (1991).
3. Holmes, K. C., Popp, D., Gebhard, W. & Kabsch, W. Atomic model of the actin filament. *Nature* **347**, 44-49 (1990).
4. Sheterline, P., Clayton, J. & Sparrow, J. Actin. *Protein Profile* **2**, 1-103 (1995).
5. Mogilner, A. & Oster, G. Cell motility driven by actin polymerization. *Biophys. J.* **71**, 3030-3045 (1996).
6. Miyata, H., Nishiyama, S., Akashi, K. & Kinosita, K. Jr Protrusive growth from giant liposomes driven by actin polymerization. *Proc. Natl Acad. Sci. USA* **96**, 2048-2053 (1999).
7. Lauffenburger, D. A. & Horwitz, A. F. Cell migration: a physically integrated molecular process. *Cell* **84**, 359-369 (1996).
8. Mitchison, T. J. & Cramer, L. P. Actin-based cell motility and cell locomotion. *Cell* **84**, 371-379 (1996).
9. Nabi, I. R. The polarization of the motile cell. *J. Cell Sci.* **112**, 1803-1811 (1999).
10. Oliver, T., Lee, J. & Jacobson, K. Forces exerted by locomoting cells. *Semin. Cell Biol* **5**, 139-147 (1994).
11. Elson, E. L., Felder, S. F., Jay, P. Y., Kolodney, M. S. & Pasternak, C. Forces in cell locomotion. *Biochem. Soc. Symp.* **65**, 299-314 (1999).
12. Dramsi, S. & Cossart, P. Intracellular pathogens and the actin cytoskeleton. *Annu. Rev. Cell Dev. Biol.* **14**, 137-166 (1998).
13. Tilney, L. G. & Portnoy, D. A. Actin filaments and the growth, movement, and spread of the intracellular bacterial parasite, *Listeria monocytogenes*. *J. Cell Biol.* **109**, 1597-1608 (1989).
14. Theriot, J. A., Mitchison, T. J., Tilney, L. G. & Portnoy, D. A. The rate of actin-based motility of intracellular *Listeria monocytogenes* equals the rate of actin polymerization. *Nature* **357**, 257-260 (1992).
15. Dabiri, G. A., Sanger, J. M., Portnoy, D. A. & Southwick, F. S. *Listeria monocytogenes* moves rapidly through the host-cell cytoplasm by inducing directional actin assembly. *Proc. Natl Acad. Sci. USA* **87**, 6068-6072 (1990).
16. Sanger, J. M., Sanger, J. W. & Southwick, F. S. Host cell actin assembly is necessary and likely to provide the propulsive force for intracellular movement of *Listeria monocytogenes*. *Infect. Immun.* **60**, 3609-3619 (1992).
17. Kocks, C. *et al.* L. monocytogenes-induced actin assembly requires the actA gene product, a surface protein. *Cell* **68**, 521-531 (1992).
18. Welch, M. D., Rosenblatt, J., Skoble, J., Portnoy, D. A. & Mitchison, T. J. Interaction of human Arp2/3 complex and the *Listeria monocytogenes* ActA protein in actin filament nucleation. *Science* **281**, 105-108 (1998).
19. Smith, G. A., Theriot, J. A. & Portnoy, D. A. The tandem repeat domain in the *Listeria monocytogenes* ActA protein controls the rate of actin-based motility, the percentage of moving bacteria, and the localization of vasodilator-stimulated phosphoprotein and profilin. *J. Cell Biol.* **135**, 647-660 (1996).
20. Kocks, C., Hellio, R., Gounon, P., Ohayon, H. & Cossart, P. Polarized distribution of *Listeria monocytogenes* surface protein ActA at the site of directional actin assembly. *J. Cell Sci.* **105**, 699-710 (1993).
21. Theriot, J. A., Rosenblatt, J., Portnoy, D. A., Goldschmidt-Clermont, P. J. & Mitchison, T. J. Involvement of profilin in the actin-based motility of *L. monocytogenes* in cells and in cell-free extracts. *Cell* **76**, 505-517 (1994).
22. Cameron, L. A., Footer, M. J., van Oudenaarden, A. & Theriot, J. A. Motility of ActA protein-coated microspheres driven by actin polymerization. *Proc. Natl Acad. Sci. USA* **96**, 4908-4913 (1999).
23. Dold, F. G., Sanger, J. M. & Sanger, J. W. Intact alpha-actinin molecules are needed for both the assembly of actin into the tails and the locomotion of *Listeria monocytogenes* inside infected cells. *Cell Motil. Cytoskeleton* **28**, 97-107 (1994).
24. Pollard, T. D. Rate constants for the reactions of ATP- and ADP-actin with the ends of actin filaments. *J. Cell Biol.* **103**, 2747-2754 (1986).
25. Hill, T. L. & Kirschner, M. W. Bioenergetics and kinetics of microtubule and actin filament assembly-disassembly. *Int. Rev. Cytol.* **78**, 1-125 (1982).
26. Yasar, D., To, W., Abo, A. & Welch, M. D. The Wiskott-Aldrich syndrome protein directs actin-based

- motility by stimulating actin nucleation with the Arp2/3 complex. *Curr. Biol.* **9**, 555–558 (1999).
27. Ma, L., Cantley, L. C., Janmey, P. A. & Kirschner, M. W. Corequirement of specific phosphoinositides and small GTP-binding protein Cdc42 in inducing actin assembly in *Xenopus* egg extracts. *J. Cell Biol.* **140**, 1125–1136 (1998).
28. Coates, T. D., Watts, R. G., Hartman, R. & Howard, T. H. Relationship of F-actin distribution to development of polar shape in human polymorphonuclear neutrophils. *J. Cell Biol.* **117**, 765–774 (1992).
29. Euteneuer, U. & Schliwa, M. Persistent, directional motility of cells and cytoplasmic fragments in the absence of microtubules. *Nature* **310**, 58–61 (1984).
30. Verkhovskiy, A. B., Svitkina, T. M. & Borisy, G. G. Self-polarization and directional motility of cytoplasm. *Curr. Biol.* **9**, 11–20 (1999).
31. Gerhart, J. *et al.* Cortical rotation of the *Xenopus* egg: consequences for the anteroposterior pattern of embryonic dorsal development. *Development* **107**, 37–51 (1989).
32. Theriot, J. A. & Fung, D. C. *Listeria monocytogenes*-based assays for actin assembly factors. *Methods Enzymol.* **298**, 114–122 (1998).
33. Doi, M. & Edwards, S. *The Theory of Polymer Dynamics* (Oxford Univ. Press, New York, 1986).
34. Yanagida, T., Nakase, M., Nishiyama, K. & Oosawa, F. Direct observation of motion of single F-actin filaments in the presence of myosin. *Nature* **307**, 58–60 (1984).
35. Ott, A., Magnasco, M., Simon, A. & Libchaber, A. Measurement of the persistence length of polymerized actin using fluorescence microscopy. *Phys. Rev. E* **48**, R1642–R1645 (1993).
36. Riveline, D., Wiggins, C. H., Goldstein, R. E. & Ott, A. Elastohydrodynamic study of actin filaments using fluorescence microscopy. *Phys. Rev. E* **56**, R1330–R1333 (1997).
37. Marchand, J. B. *et al.* Actin-based movement of *Listeria monocytogenes*: actin assembly results from the local maintenance of uncapped filament barbed ends at the bacterium surface. *J. Cell Biol.* **130**, 331–343 (1995).
38. Laine, R. O. *et al.* Gelsolin, a protein that caps the barbed ends and severs actin filaments, enhances the actin-based motility of *Listeria monocytogenes* in host cells. *Infect. Immun.* **66**, 3775–3782 (1998).

ACKNOWLEDGEMENTS

We thank L. Cameron for providing purified ActA–His protein for the experiment shown in Fig. 1, and K. Lustig, J. Robbins, K. Jung, L. Cameron, S. McCallum and P. Giardini for comments on the manuscript. This work was supported by grants from the NIH (AI36929) and the David and Lucile Packard Foundation to J.A.T., and from the Dutch Organization for Scientific Research (NWO) to A.v.O. Correspondence and requests for materials should be addressed to J.A.T.